

Karol Mikula · Alessandro Sarti · Fiorella Sgallari

# Co-volume method for Riemannian mean curvature flow in subjective surfaces multiscale segmentation

Received: 19 September 2002 / Accepted: 18 April 2005 / Published online: 21 February 2006  
 © Springer-Verlag 2006

**Abstract** We introduce semi-implicit complementary volume numerical scheme for solving the level set formulation of Riemannian mean curvature flow problem arising in image segmentation, edge detection, missing boundary completion and subjective contour extraction. The scheme is robust and efficient since it is linear, and it is stable in  $L_\infty$  and weighted  $W^{1,1}$  sense without any restriction on a time step. The computational results related to medical image segmentation with partly missing boundaries and subjective contours extraction are presented.

**Keywords** Partial differential equations · Nonlinear diffusion · Riemannian mean curvature flow · Level set formulation · Complementary volume method · Semi-implicit scheme · Image segmentation · Edge detection · Subjective contours · Subjective surfaces · Medical imaging

## 1 Introduction

In this paper we introduce and study linear numerical scheme for solving nonlinear degenerate diffusion equation arising in image segmentation and edge detection, computer and human vision. Our scheme is based on semi-implicit approximation in time and on the so-called complementary volume method in space. We study discretization of nonlin-

ear degenerate diffusion equation of Riemannian mean curvature flow type [4, 16, 22]

$$u_t = |\nabla u| \nabla \cdot \left( g(|\nabla G_\sigma * I^0|) \frac{\nabla u}{|\nabla u|} \right), \quad (1)$$

where  $u(t, x)$  is an unknown (segmentation) function defined in  $Q_T \equiv [0, T] \times \Omega$ ,  $\Omega \subset \mathbb{R}^d$  is a bounded rectangular domain,  $[0, T]$  is a time interval, and  $I^0$  is a given image. The equation is accompanied with zero Dirichlet boundary condition and initial condition

$$u = 0 \quad \text{on } [0, T] \times \partial\Omega, \quad (2)$$

$$u(0, x) = u^0(x) \quad \text{in } \Omega. \quad (3)$$

The assumptions on the data in (1)-(3) are as follows:

$g : \mathbb{R}_0^+ \rightarrow \mathbb{R}^+$  is a decreasing function,  $g(\sqrt{s})$  is smooth,  $g(0) = 1$ ,  $g(s) \rightarrow 0$  for  $s \rightarrow \infty$  [20],

$G_\sigma \in C^\infty(\mathbb{R}^d)$  is a smoothing kernel (e.g. Gauss function),

$$\text{with } \int_{\mathbb{R}^d} G_\sigma(x) dx = 1, \int_{\mathbb{R}^d} |\nabla G_\sigma| dx \leq C_\sigma, \quad (5)$$

$G_\sigma(x) \rightarrow \delta_x$  for  $\sigma \rightarrow 0$ ,  $\delta_x$  is the Dirac measure at point  $x$ ,

$$u^0 \in L_\infty(\Omega), \quad (6)$$

and

$$\nabla G_\sigma * I^0 = \int_{\mathbb{R}^d} \nabla G_\sigma(x - \xi) \tilde{I}^0(\xi) d\xi, \quad (7)$$

where  $\tilde{I}^0$  is extension of  $I^0$  to  $\mathbb{R}^d$  given by periodic reflection through boundary of  $\Omega$ .

Equations of weighted mean curvature flow type have been successively introduced to image segmentation and edge detection by several groups in the last decade [4, 5, 16, 22–24]. Besides segmentation, the nonlinear PDEs related to mean curvature motion are often used also in image filtration. e.g., the equation

$$u_t - g(|\nabla G_\sigma * u|) |\nabla u| \nabla \cdot \left( \frac{\nabla u}{|\nabla u|} \right) = 0 \quad (8)$$

Communicated by: G. Wittum

K. Mikula (✉)

Department of Mathematics, Slovak University of Technology, Radlinského 11, 813 68 Bratislava, Slovakia  
 E-mail: mikula@vox.svf.stuba.sk

A. Sarti

DEIS, University of Bologna, Via Risorgimento 2, 40136 Bologna, Italy  
 E-mail: asarti@deis.unibo.it

F. Sgallari

Department of Mathematics, University of Bologna, Piazza di Porta S. Donato 5, 40127 Bologna, Italy  
 E-mail: sgallari@dm.unibo.it

has been suggested in [2] for image selective smoothing based on morphological principle and isophotes information. In [7], the diffusion weighting term  $g(|\nabla G_\sigma * I^0|)$  of (1) is changed to adaptively updated one  $g(|\nabla G_\sigma * u|)$ , and such model is again used for nonlinear image filtration. In particular case  $g \equiv 1$ , (1) and (8) reduce to the well-known level set equation [19, 25] moving all level sets of  $u$  by the normal mean curvature field. It is used in wide range of applications related to front propagation and interphase motions in free boundary problems; for a comprehensive overview we refer to [26]. Study of the existence of unique viscosity solution to all these types of degenerate parabolic equations is based on [6, 8, 12].

In image filtration, the initial condition for Eq. (8) is given by the image greylevel intensity  $I^0$  itself, i.e.  $u^0 = I^0$ . Then the solution  $u(t, x)$  of (8) gives a family of *scaled* (filtered, smoothed) versions of  $I^0(x)$ . The parameter  $t$  is understood as *scale*, and the process of nonlinear selective smoothing is called image multiscale analysis [1]. In [13], the linear complementary volume method to solve image selective smoothing Eq. (8) has been suggested and studied.

In image segmentation and edge detection which we are going to deal with in this paper, the initial condition  $u^0(x)$  represents an initial state of the so-called segmentation function  $u(t, x)$ . The image  $I^0$  determines the weight function  $g$  for the mean curvature motion of level sets of the segmentation function. Equation (1) can be rewritten as

$$u_t = g(|\nabla G_\sigma * I^0|) |\nabla u| \nabla \cdot \left( \frac{\nabla u}{|\nabla u|} \right) + \nabla g(|\nabla G_\sigma * I^0|) \cdot \nabla u. \quad (9)$$

The vector field  $\nabla g$  drives level sets of the segmentation function  $u$  towards edges in the image [4, 16]. The second order regularization term, first on the right hand side, filters the evolving segmentation function from stopping on spurious edges [2]. Moreover, this degenerate diffusion term close the edges with missing large gradient information as in subjective contour case ([22]; see also numerical examples in Sect. 3 of this paper).

In the above mentioned literature, one can find a discretization of (1) based on the form (9) and explicit schemes with an upwinding for convective term are often used. Then a stability restriction on the time stepping has to be imposed. In this paper, we discretize the form (1) using semi-implicit complementary volume method which gives unconditionally stable scheme in  $L_\infty$  and weighted  $W^{1,1}$  sense without any restriction on the time step. The scheme is linear at every discrete time step, so one can get fast CPU times, either using preconditioned linear iterative solvers [13, 17, 21] or approximate additive operator splitting approach [28].

The method presented in this paper is based on the results developed in [13]. However, one should also notice important differences. Here, we study different field of application, not the image smoothing but the image segmentation. In spite of image smoothing where usually zero

Neumann boundary conditions are used, in image segmentation Dirichlet boundary data are considered. The structure of the models (1) and (8) is different. In (1) the weighting term  $g$  is inside the divergence which brings new convective phenomenon into the model important in segmentation context. In spite of the previous methods dealing with (1), we employ directly its divergence structure without going to equivalent form (9), which is the main reason why the semi-implicit co-volume method can be used efficiently also for solving PDEs arising in image segmentation.

The rest of this paper is organized as follows. In Sect. 2 we present our discretization of (1) in the context of image segmentation and we prove stability properties of such numerical approximation. In Sect. 3, we present numerical experiments in edge detection for objects with partly missing boundaries, e.g. in extraction of subjective contours and segmentation of echocardiographic images.

## 2 Linear semi-implicit complementary volume scheme

In order to discretize (1) we have chosen  $N \in \mathbb{N}$  and set a uniform discrete time step  $\tau = \frac{T}{N}$ . Then we replace the time derivative in (1) by backward difference and the nonlinear terms of equation are treated from the previous time step while the linear ones are considered on the current time level (for other semi-implicit approaches in image processing we refer, e.g., to [3, 13, 15, 18, 28]). We denote

$$g^0 := g(|\nabla G_\sigma * I^0|), \quad (10)$$

for which

$$g^0 \geq \nu_\sigma > 0$$

holds due to smoothing properties of the convolution [2, 15]. Then we can formally write the semi-discrete in time discretization of (1):

Let  $N \in \mathbb{N}$ ,  $\tau = \frac{T}{N}$  and  $\sigma > 0$  be fixed numbers,  $I^0$  be a given image and  $u^0$  be a given initial segmentation function. Then, for  $n = 1, \dots, N$ , we look for a function  $u^n$ , solution of the equation

$$\frac{1}{|\nabla u^{n-1}|} \frac{u^n - u^{n-1}}{\tau} = \nabla \cdot \left( g^0 \frac{\nabla u^n}{|\nabla u^{n-1}|} \right). \quad (11)$$

Since the denominators of (11) can vanish, we will regularize them in the sense of Evans and Spruck [12]. Presize formulation of the regularization and properties of such solutions will be given below in a description of fully discrete scheme.

In the segmentation tasks, a discrete image is usually given on a rectangular structure of pixels. For such discrete image, as the input of the segmentation method based on (1) we have to compute at the beginning the parameter  $g^0$ . The input  $g^0$  represents the Perona-Malik function applied

to (smoothed) gradient of the discrete image intensity. Moreover, at every discrete time step of the method (11) we have to evaluate  $|\nabla u^{n-1}|$ , the absolute value of the solution gradient at the previous time level. Since in both cases we work with the gradient of the image  $I^0$  and with the gradient of the solution  $u^{n-1}$ , it is reasonable to put a triangulation onto the image domain and then evaluate the gradients of their piecewise linear representations on the triangulation. Such approach gives constant values for the computed quantities per triangles and thus it allows very simple construction of linear systems to be solved. It is a key feature of the complementary volume [13, 27] and finite element (see e.g. [9–11]) methods for solving mean curvature flow problems. Since the model contains an image information given by  $g^0$ , we use a specific triangulation respecting the pixel structure of the image (solid lines in Fig. 1). The centers of pixels correspond to the nodes of such triangulation. Then we connect these nodes by a new rectangular mesh and further split every new rectangle into two triangles (see dashed lines in Fig. 1 representing our triangular grid). The computational domain  $\Omega$  in (1)–(3) is then the union of these triangles, i.e., the image domain minus outer half of every boundary pixel. Of course, if one wants to segment only a part of the image where the object to be segmented is located, the triangulation is constructed only in a corresponding smaller part of the image domain. Let us also note that it is not necessary to consider only one orientation of triangles as in Fig. 1. From practical point of view, we have good experience with an averaging of computational results using both triangle orientations.

In complementary volume method, together with a triangulation  $\mathcal{T}_h$  (given, e.g., by the previous construction) also the so-called dual mesh is used [27]. The dual mesh consists of cells  $V_i$  (called also complementary volumes, control volumes or co-volumes) associated with the  $i$ th inner node,  $i = 1, \dots, M$ , of triangulation  $\mathcal{T}_h$  (we exclude boundary nodes for which zero value is prescribed due to Dirichlet boundary condition). The co-volume  $V_i$  is bounded by the lines that bisect and are perpendicular to the edges emanating from the node. Let us note, that in our case the dual mesh again corresponds to the pixel structure of the image, it covers all pixels besides the boundary ones.

We will denote the edge of  $\mathcal{T}_h$  connecting the  $i$ th node to the  $j$ th by  $\sigma_{ij}$  and its length by  $h_{ij}$ . We denote by  $\mathcal{E}_{ij}$  the set of simplices having  $\sigma_{ij}$  as an edge, i.e.,  $\mathcal{E}_{ij} = \{T \in \mathcal{T}_h | \sigma_{ij} \subset T\}$ . Let  $e_{ij}$  denote the co-edge that is perpendicular bisector of  $\sigma_{ij}$ . For each  $T \in \mathcal{E}_{ij}$  let  $c_{ij}^T$  be the length of the portion of  $e_{ij}$  that is in  $T$ , i.e.,  $c_{ij}^T = |e_{ij} \cap T|$ . For each node of  $\mathcal{T}_h$  let  $C_i$  denote the set of nodes connected to the  $i$ th node by an edge.

Given a triangulation  $\mathcal{T}_h$ , we define the set  $V_h$  of continuous piecewise linear functions fulfilling (2), i.e.,  $V_h = V_h(\mathcal{T}_h) := \{v \in C^0(\Omega) | v|_T \in \mathcal{P}_1 \text{ for all } T \in \mathcal{T}_h, v|_{\partial\Omega} = 0\}$ . Then  $|\nabla u_h|$ ,  $u_h \in V_h$  has a constant value on every triangle  $T \subset \mathcal{T}_h$ . We will denote that value by  $|\nabla u_T|$ . For any  $u_h \in V_h$  we will use notation  $u_i := u_h(x_i)$  where  $x_i$  is  $i$ th node of triangulation. Let  $\mathcal{N}_i$  be the set of simplices that have

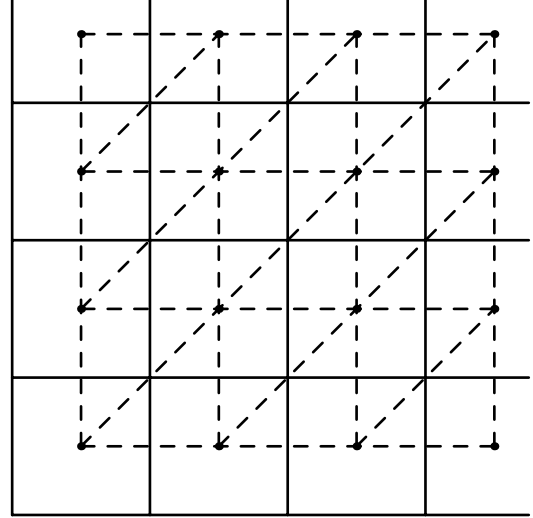


**Fig. 1** The image pixels (solid lines) corresponding to the dual mesh for complementary volume method. Triangulation (dashed lines) for the complementary volume method with nodes (round points) corresponding to centers of pixels

the  $i$ th node as a vertex. Let  $u_h^0 = I_h(u^0) \in V_h$  be the nodal interpolant of  $u^0$ . Let  $\varepsilon > 0$ . For any  $u_h \in V_h$  we define

$$|\nabla u_h|_\varepsilon = \sqrt{\varepsilon^2 + |\nabla u_h|^2} \quad (12)$$

and then for any  $T \subset \mathcal{T}_h$

$$|\nabla u_T|_\varepsilon = \sqrt{\varepsilon^2 + |\nabla u_T|^2}. \quad (13)$$

With these notations we are ready to derive the fully discrete complementary volume spatial discretization and to state some of its properties. First we integrate (11) over a co-volume  $V_i$ ,  $i = 1, \dots, M$ ,

$$\int_{V_i} \frac{u^n - u^{n-1}}{|\nabla u^{n-1}|_\tau} dx = \int_{V_i} \nabla \cdot \left( g^0 \frac{\nabla u^n}{|\nabla u^{n-1}|} \right) dx, \quad (14)$$

and then for the right hand side we use the divergence theorem to get

$$\int_{V_i} \nabla \cdot \left( g^0 \frac{\nabla u^n}{|\nabla u^{n-1}|} \right) dx = \sum_{j \in C_i} \int_{e_{ij}} \frac{g^0}{|\nabla u^{n-1}|} \frac{\partial u^n}{\partial \nu} ds. \quad (15)$$

If  $u_h^n \in V_h$  and  $I_h^\sigma$  (approximation of  $I^\sigma \equiv G_\sigma * I^0$ ) are continuous piecewise linear functions on triangulation  $\mathcal{T}_h$  then we can continue by

$$\begin{aligned} & \sum_{j \in C_i} \int_{e_{ij}} \frac{g^0}{|\nabla u_h^{n-1}|} \frac{\partial u_h^n}{\partial \nu} ds \\ &= \sum_{j \in C_i} \left( \sum_{T \in \mathcal{E}_{ij}} c_{ij}^T \frac{g(|\nabla I_T^\sigma|)}{|\nabla u_T^{n-1}|} \right) \frac{u_j^n - u_i^n}{h_{ij}}. \end{aligned} \quad (16)$$

Using the approach of [27], the left hand side of (14) is approximated by the term

$$\frac{|V_i|(u_i^n - u_i^{n-1})}{\tau |\nabla u_i^{n-1}|} \quad (17)$$

where  $|\nabla u_i^{n-1}|$  denotes an approximation of the gradient of  $u^{n-1}$  in the co-volume  $V_i$  for which the weighted average is chosen, i.e. for any  $u_h \in V_h$  we define

$$|\nabla u_i| = \sum_{T \in \mathcal{N}_i} \frac{|T \cap V_i|}{|V_i|} |\nabla u_T| \quad (18)$$

and the regularization is given by

$$|\nabla u_i|_\varepsilon = \sum_{T \in \mathcal{N}_i} \frac{|T \cap V_i|}{|V_i|} |\nabla u_T|_\varepsilon. \quad (19)$$

Then we define coefficients

$$b_i^{n-1} = \frac{|V_i|}{|\nabla u_i^{n-1}|_\varepsilon}, \quad (20)$$

$$a_{ij}^{n-1} = \frac{1}{h_{ij}} \sum_{T \in \mathcal{E}_{ij}} c_{ij}^T \frac{g(|\nabla I_T^\sigma|)}{|\nabla u_T^{n-1}|_\varepsilon}. \quad (21)$$

The coefficient (21) includes evaluation of  $|\nabla I_T^\sigma|$ . For that goal, before the first time step, we use a strategy which is natural for the complementary volume method (see also [3]). Using the Gauss function (fundamental solution of the heat equation) as smoothing kernel  $G_\sigma$  one can replace the term  $G_\sigma * I^0$  by solving the linear heat equation for time  $\sigma$  with initial datum given by  $I^0$ . This linear equation is solved numerically at the same grid by just one implicit time step. Thus we look for a function  $I^\sigma$  which is solution of

$$\frac{I^\sigma - I^0}{\sigma} = \Delta I^\sigma \quad (22)$$

where  $\Delta$  denotes Laplace operator. The discrete piecewise linear approximation  $I_h^\sigma$  on triangulation  $\mathcal{T}_h$ , is found by the same approach as given in (14)–(17) applied to Eq. (22) with zero Neumann conditions at the boundary of image domain. On one side, the convolution with smoothing kernel represents a preliminary smoothing of the data. On the other hand, it is a theoretical tool to have bounded gradients and thus a strictly positive weighting coefficient  $g^0$ . In practice, the evaluation of gradients on discrete grid (e.g., on triangulation described above) gives always bounded values. So one can also avoid (22) if no preliminary denoising is needed and work directly with  $I_h^0$  and with values  $|\nabla I_T^0|$  in (21). Using (16) and (17) together with definitions (20), (21) we can write the scheme.

### Linear semi-implicit fully discrete complementary volume scheme for solving Eq. (1):

For  $n = 1, \dots, N$  we look for  $u_i^n, i = 1, \dots, M$ , satisfying

$$b_i^{n-1}(u_i^n - u_i^{n-1}) + \tau \sum_{j \in C_i} a_{ij}^{n-1}(u_i^n - u_j^n) = 0. \quad (23)$$

The solution  $(u_1^n, \dots, u_M^n)$  to the linear system (23) will be denoted by  $u_h^{\varepsilon, n}$ . We have the following assertion for  $u_h^{\varepsilon, n}$  and also for a generalized solution of the scheme, i.e. for a limit of  $u_h^{\varepsilon, n}$  when  $\varepsilon \rightarrow 0$ . For  $u_h \in V_h$  let  $\|\nabla u_h\|_{L_{1,g}(\Omega)} = \int_\Omega g_h^0 |\nabla u_h| dx$ ,  $g_h^0 = g(|\nabla I_h^\sigma|)$  denote the weighted  $L_1$  norm of the gradient.

**Theorem.** *There exists unique solution  $u_h^{\varepsilon, n} = (u_1^n, \dots, u_M^n)$  of the scheme (23) for any  $\varepsilon > 0, n = 1, \dots, N$ . Moreover, there exists a generalized solution of the scheme, i.e. a limit  $u_h^n$  of a subsequence of  $u_h^{\varepsilon, n}$  for  $\varepsilon \rightarrow 0$  for which following stability estimates hold*

$$\begin{aligned} \|u_h^n\|_{L_\infty(\Omega)} &\leq \|u_h^0\|_{L_\infty(\Omega)}, \\ \|\nabla u_h^n\|_{L_{1,g}(\Omega)} &\leq \|\nabla u_h^0\|_{L_{1,g}(\Omega)}, \quad 1 \leq n \leq N. \end{aligned} \quad (24)$$

*Proof.* The scheme (23) gives the linear system with a symmetric and diagonally dominant M-matrix which guarantee its unique solution. Moreover, the positiveness of the diagonal and negativeness of the off-diagonal coefficients imply fulfilling of the discrete minimum-maximum principle for the scheme (23) which gives for any  $\varepsilon > 0$

$$\|u_h^{\varepsilon, n}\|_{L_\infty(\Omega)} \leq \|u_h^0\|_{L_\infty(\Omega)}, \quad 1 \leq n \leq N. \quad (25)$$

Since estimate (25) is independent on  $\varepsilon$  we can choose convergent subsequence of  $u_h^{\varepsilon, n}$  as  $\varepsilon \rightarrow 0$ . The limit  $u_h^n \in V_h$  of this subsequence then clearly fulfills the first estimate of the Theorem.

If we multiply (23) by  $u_i^n - u_i^{n-1}$  and sum it over all nodes, we get

$$\begin{aligned} \sum_{i=1}^M b_i^{n-1} \frac{(u_i^n - u_i^{n-1})^2}{\tau} \\ + \sum_{i=1}^M \sum_{j \in C_i} a_{ij}^{n-1} (u_i^n - u_j^n)(u_i^n - u_i^{n-1}) = 0. \end{aligned} \quad (26)$$

If  $\mathcal{T}_h$  is a two-dimensional mesh having triangles with interior angles not exceeding  $\pi/2$  and if  $u, v \in V_h$ , and  $w$  is piecewise constant on  $\mathcal{T}_h$ , then

$$\int_\Omega w \nabla u \cdot \nabla v dx = \sum_{i=1}^{\overline{M}} \left( \sum_{j \in C_i} \alpha_{ij}(w)(u_i - u_j) \right) v_i, \quad (27)$$

where  $\alpha_{ij}(w) = \frac{1}{h_{ij}} \sum_{T \in \mathcal{E}_{ij}} w_T c_{ij}^T$ ,  $w_T$  denotes value of  $w$  in

$T \in \mathcal{T}_h$  and  $\overline{M}$  is number of nodes in triangulation  $\mathcal{T}_h$  (see e.g. [27]). Since  $v_i$  is zero for boundary nodes, we can replace  $\overline{M}$  by  $M$  and using definition of  $a_{ij}^{n-1}$  we obtain

$$\begin{aligned} \sum_{i=1}^M b_i^{n-1} \frac{(u_i^n - u_i^{n-1})^2}{\tau} \\ + \int_\Omega g_h^0 \frac{\nabla u_h^{\varepsilon, n} \cdot \nabla (u_h^{\varepsilon, n} - u_h^{n-1})}{|\nabla u_h^{n-1}|_\varepsilon} dx = 0. \end{aligned} \quad (28)$$

Then the second term is equal to

$$\int_{\Omega} g_h^0 \frac{\nabla u_h^{\varepsilon,n} \cdot \nabla (u_h^{\varepsilon,n} - u_h^{n-1})}{|\nabla u_h^{n-1}|_{\varepsilon}} dx = \frac{1}{2} \int_{\Omega} g_h^0 \frac{|\nabla u_h^{\varepsilon,n}|^2 - |\nabla u_h^{n-1}|^2 + |\nabla u_h^{\varepsilon,n} - \nabla u_h^{n-1}|^2}{|\nabla u_h^{n-1}|_{\varepsilon}} dx$$

and

$$\begin{aligned} & |\nabla u_h^{\varepsilon,n} - \nabla u_h^{n-1}|^2 \\ &= (|\nabla u_h^{\varepsilon,n}| - |\nabla u_h^{n-1}|_{\varepsilon})^2 \\ &+ \left(2 - \frac{2\nabla u_h^{\varepsilon,n} \cdot \nabla u_h^{n-1}}{|\nabla u_h^{\varepsilon,n}| |\nabla u_h^{n-1}|_{\varepsilon}}\right) |\nabla u_h^{\varepsilon,n}| |\nabla u_h^{n-1}|_{\varepsilon} - \varepsilon^2. \end{aligned}$$

If we denote  $\nabla_{\varepsilon} v = (v_x, v_y, \varepsilon)$ , and  $\nabla_0 v = (v_x, v_y, 0)$ , where  $v_x, v_y$  denote partial derivatives of a function  $v$ , we get from (28)

$$\begin{aligned} & \sum_{i=1}^M b_i^{n-1} \frac{(u_i^n - u_i^{n-1})^2}{\tau} \\ &+ \int_{\Omega} g_h^0 \frac{(|\nabla u_h^{\varepsilon,n}| - |\nabla u_h^{n-1}|_{\varepsilon})^2}{|\nabla u_h^{n-1}|_{\varepsilon}} dx \\ &+ \frac{1}{2} \int_{\Omega} g_h^0 \left| \frac{\nabla_0 u_h^{\varepsilon,n}}{|\nabla_0 u_h^{\varepsilon,n}|} - \frac{\nabla_{\varepsilon} u_h^{n-1}}{|\nabla_{\varepsilon} u_h^{n-1}|} \right|^2 |\nabla u_h^{\varepsilon,n}| dx \\ &+ \frac{1}{2} \int_{\Omega} g_h^0 \frac{|\nabla u_h^{\varepsilon,n}|^2 - |\nabla u_h^{n-1}|_{\varepsilon}^2 - (|\nabla u_h^{\varepsilon,n}| - |\nabla u_h^{n-1}|_{\varepsilon})^2}{|\nabla u_h^{n-1}|_{\varepsilon}} dx \\ &= 0. \end{aligned}$$

Due to positiveness of the first three terms we have

$$\frac{1}{2} \int_{\Omega} g_h^0 \frac{2|\nabla u_h^{\varepsilon,n}| |\nabla u_h^{n-1}|_{\varepsilon} - 2|\nabla u_h^{n-1}|_{\varepsilon}^2}{|\nabla u_h^{n-1}|_{\varepsilon}} dx \leq 0$$

which imply that

$$\begin{aligned} \int_{\Omega} g_h^0 |\nabla u_h^{\varepsilon,n}| dx &\leq \int_{\Omega} g_h^0 |\nabla u_h^{n-1}|_{\varepsilon} dx \\ &= \int_{\Omega} g_h^0 \sqrt{|\nabla u_h^{n-1}|^2 + \varepsilon^2} dx \\ &\leq \int_{\Omega} g_h^0 |\nabla u_h^{n-1}| dx + \varepsilon \int_{\Omega} g_h^0 dx \\ &\leq \int_{\Omega} g_h^0 |\nabla u_h^{n-1}| dx + \varepsilon |\Omega| \end{aligned} \quad (29)$$

hold for any  $\varepsilon > 0$ . Let  $u_h^{\varepsilon,n}$  be the subsequence converging to  $u_h^n$  as  $\varepsilon \rightarrow 0$  and the corresponding vector be  $u_h^n = (u_{h,1}^n, u_{h,2}^n, \dots, u_{h,M}^n)$ . Then there exists a subsequence of the previous one for which  $|\nabla u_T^{\varepsilon,n}| \rightarrow |\nabla u_T^n|$ ,  $\forall T \in \mathcal{T}_h$  as  $\varepsilon \rightarrow 0$  and so  $\|\nabla u_h^{\varepsilon,n}\|_{L^{1,g}(\Omega)} \rightarrow \|\nabla u_h^n\|_{L^{1,g}(\Omega)}$  for  $\varepsilon \rightarrow 0$ . From (29) then follows the second estimate of the Theorem.

*Remark.* In [27], Walkington used the following "implicit" nonlinear semi-discretization in time

$$\frac{1}{|\nabla u^n| + |\nabla u^{n-1}|} \frac{u^n - u^{n-1}}{\tau} - \nabla \cdot \left( \frac{\nabla u^n}{|\nabla u^n| + |\nabla u^{n-1}|} \right) = 0 \quad (30)$$

for the mean curvature flow in the level set formulation. There, the averaging of gradient term from previous and current time step is considered in denominators. Such scheme after co-volume spatial discretization leads to  $L_{\infty}$  and  $W^{1,1}$  estimates as proven in [27]; our work has been inspired by that paper. Similarly to the mean curvature motion, for the equation (1) a decay of *weighted total variation* is the basic property. To see it, one can multiply the equation by a test function  $v$ , integrate it over  $\Omega$ , then take  $v = u_t$  and use  $\frac{d}{dt} |\nabla u| = \frac{\nabla u}{|\nabla u|} \nabla u_t$ . One gets

$$\int_{\Omega} \frac{(u_t)^2}{|\nabla u|} dx + \frac{d}{dt} \int_{\Omega} g^0 |\nabla u| dx = 0,$$

which means that the weighted  $L_1$  norm of the gradient is decreasing in time. As pointed out in [27], the numerical approximations should also respect this fact. The "implicit" approach by Walkington would give such property also for the solution to equation (1), but such a scheme would yield nonlinear algebraic systems in discrete time steps. Newton's like methods have no guarantee to converge [27] and other possibilities like fixed point nonlinear iterations are very slow. Our linear scheme seems to be optimal regarding stability properties and efficiency of computations.

*Remark.* The statement (27) indicates the relation between co-volume and (linear) finite element methods. In fact, for the triangulation and the co-volumes considered here (see Fig. 1) one can easily compare the methods. The finite element method with standard linear Lagrangean bases functions gives the stiffness matrix exactly corresponding to the second term of (23). Of course, the consistent finite element mass matrix is nondiagonal, and not with five nonzero entries in a row, but with seven. Using row-mass-lumping one can diagonalize it and on the diagonal get expression with the same structure as the first term of (23), but with

$$b_i^{n-1} = |V_i| |\nabla u_i^{n-1}|_{\varepsilon}$$

where

$$|\nabla u_i|_{\varepsilon} = \sum_{T \in \mathcal{N}_i} \frac{|T \cap T_i|}{|T_i|} \frac{1}{|\nabla u_T|_{\varepsilon}}, \quad T_i = \bigcup_{T \in \mathcal{N}_i} T.$$

It is clear that also such scheme fulfills our stability estimates and it can be worth to apply the scheme also computationally.

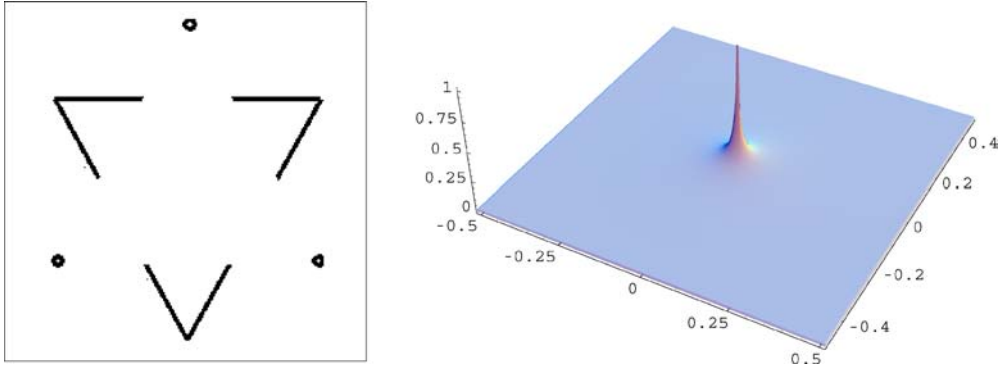


**Fig. 2** Image with subjective contours (left) and initial state of the segmentation function (right).

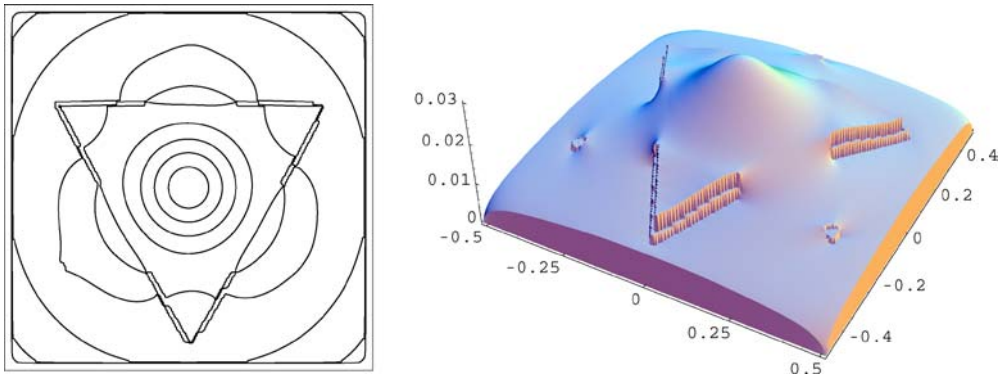


**Fig. 3** Level lines and 3D graph of the segmentation function after 10 time steps

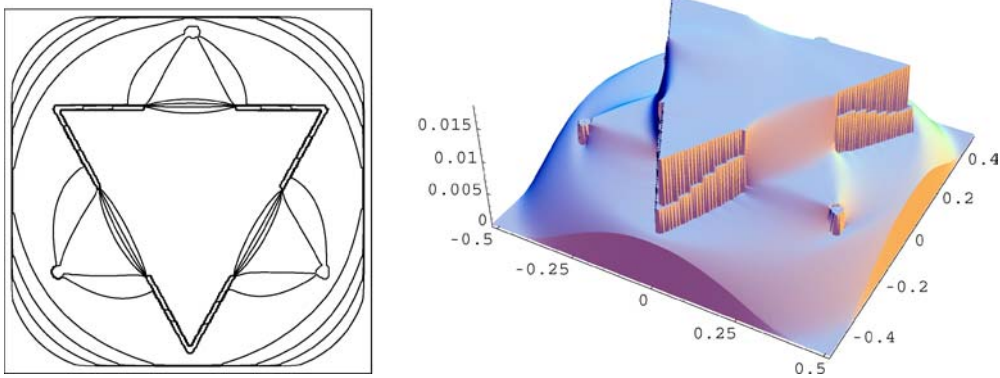


**Fig. 4** Level lines and 3D graph of the segmentation function after 50 time steps

### 3 Discussion on numerical results

This section is devoted to discussion on numerical experiments computed by the semi-implicit complementary volume scheme (23). In the presented computations we have chosen  $g(s) = \frac{1}{1+Ks^2}$  with constant  $K = 0.1$ , the regularization parameter  $\varepsilon = 10^{-5}$  for the first experiment (Fig. 2 left) and  $\varepsilon = 10^{-2}$  for the second experiment (Fig. 8 left), the convolution is omitted (i.e., we work directly with discrete image  $I_h^0$ ), time step  $\tau = 0.001$  and the space step  $h$

is given as  $\frac{1}{n_1}$ , where  $n_1, n_2$  are numbers of pixels in vertical and horizontal directions. It means, we embed the image into a rectangle  $[-0.5\frac{n_2}{n_1}, 0.5\frac{n_2}{n_1}] \times [-0.5, 0.5]$ . We start with simple initial segmentation function given as a peak centered at origin [23], as plotted in Figs. 2 and 8 right. In Figs. 2 and 8 left we present two testing images for which we want to complete contours and close the missing boundaries (subjective contours of the classic triangle of Kanizsa in the first case, and inner and outer boundary of human left ventricle in echocardiographic image in the second case).

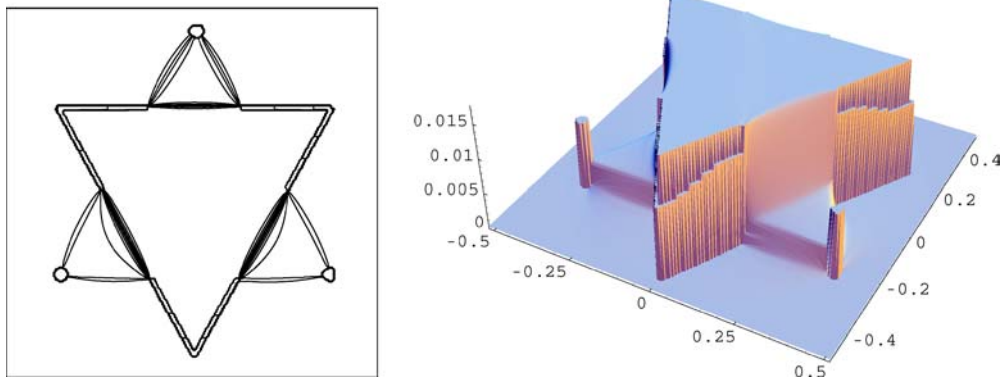


Fig. 5 Level lines and 3D graph of the segmentation function after 200 time steps

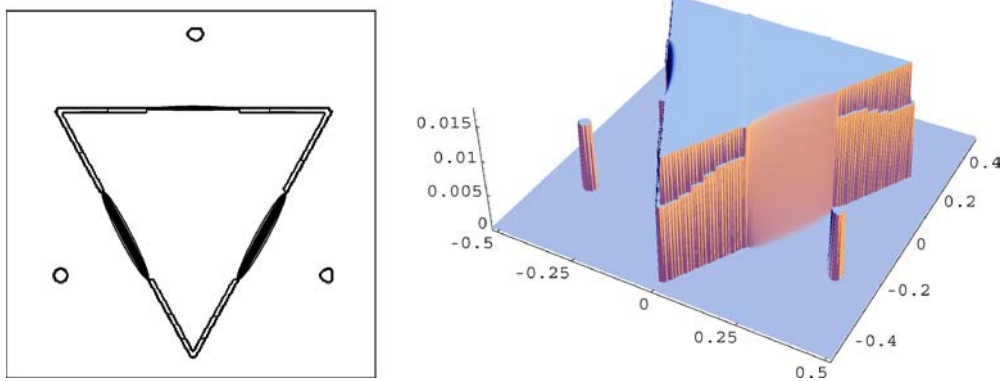


Fig. 6 Level lines and 3D graph of the segmentation function after 500 time steps

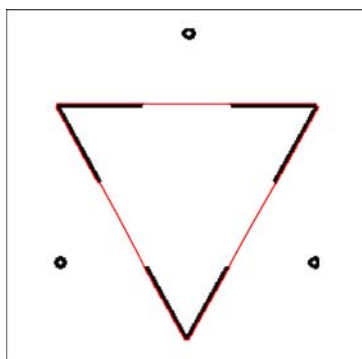
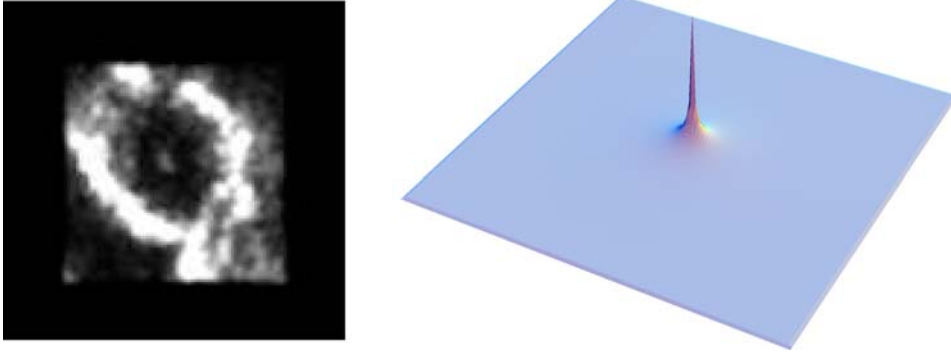


Fig. 7 Image together with extracted subjective contour

The phenomenon of contours that appear in the absence of physical gradients has aroused considerable interest among psychologists and computer vision scientists. Psychologists suggested a number of images that strongly requires image completion to detect the objects. In Fig. 2, the solid triangle in the center of the figure appears to have well defined contours, even in completely homogeneous areas. Kanizsa called the contours without gradient "subjective contours" [14], because the missed boundaries are provided by the visual system of the subject. We apply our algorithm

in order to extract the solid triangle and complete the boundaries.

For the first experiment we have given image with  $234 \times 227$  pixels. In the next subsequent figures we plot level lines (in the left) and 3D graphs (in the right) of the evolving segmentation function. The figures show the accumulation of level lines to edges (with closing of missing parts by linear segments) and the shock formations in corresponding 3D graphs. In our approach, the segmentation is a piecewise constant approximation of the image. To achieve the piecewise constant graph, an initial surface depending on the point of view is evolved with a mean curvature flow with respect to the Riemannian metric given by the image features, cf. [22]. During the evolution, the initial surface is attracted by the existing boundaries and steepens. The surface evolves towards the piecewise constant solution by continuation and closing of the boundary fragments and the filling in the homogeneous regions. A solid object is delineated as a constant surface bounded by existing and recovered shape boundaries. The theoretical basis of the method has been presented in [23] and its extension to 3D image completion has been discussed in [24]. In Fig. 7 we plot the level line closing the subjective contour (of the "first level triangle"), which is the final state of the segmentation. From computations also nicely developed boundary of the "second level



**Fig. 8** Echocardiographic image (left) and initial state of the segmentation function (right)

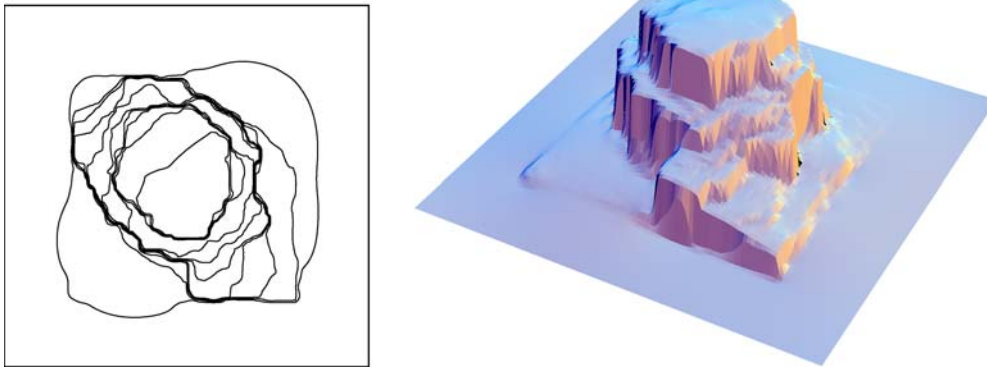


**Fig. 9** Level lines and 3D graph of the segmentation function after 50 time steps

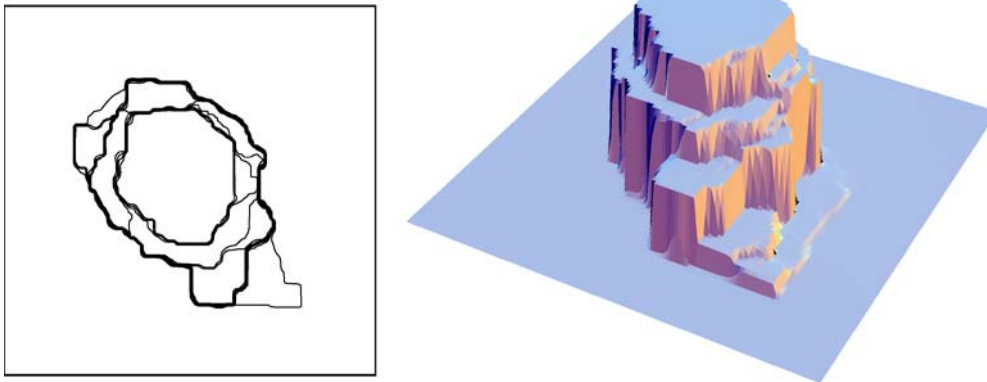


**Fig. 10** Level lines and 3D graph of the segmentation function after 500 time steps

triangle” can be observed for long period of time. The time can be understood as a scale for a multiscale edge detection process.

The second testing image is an in vivo acquired echocardiography of a left ventricle and we apply the segmentation algorithm to extract endocardiac and epicardiac boundaries. The dimension of the image is  $117 \times 117$  pixels. In Fig. 11 we plot two level lines, one close to maximum of the segmentation function, the second close to its minimum, which show inner and outer ventricular boundary.

Concerning CPU times, one step of the semi-implicit scheme takes about 0.25 sec for usual image sizes ( $256 \times 256$ ) at standard Linux PCs (2.4GHz). We run computations till the change in segmentation function is below certain threshold. For two presented experiments 500 steps were enough and we show results of this multiscale sequence. However, practically same results one can get with even bigger time step ( $\tau = 0.01$ ) with only 50 semi-implicit steps. Of course, one can use also explicit version of the co-volume scheme (23) or some other explicit approach to solve (1).

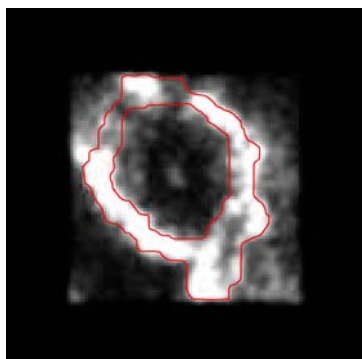


**Fig. 11** Echocardiographic image together with extracted inner and outer boundaries of the left ventricle

Then due to stability constrain, e.g., for our first image one has to consider  $\tau = 0.000001$  which would lead to unrealistic number of steps to achieve multiscale segmentation sequence. Although the explicit scheme does not solve any system, for nonlinear problems as (1), the construction of coefficients like (20)–(21) is necessary at every time step which is time consuming itself. Thus the global CPU time for such scheme is much bigger than for the semi-implicit one.

**Acknowledgements** This work was supported by NATO Collaborative Linkage Grant No. PST.CLG.979123, by grants VEGA 1/3321/06 and APVT-20-040902, by MURST grant MM01111258 and GNCS-INDAM, and by the Stefan Banach International Mathematical Centre as a Centre of Excellence at ICM, Warsaw University.

## References

1. Alvarez, L., Guichard, F., Lions, P.L., Morel, J.M.: Axioms and Fundamental Equations of Image Processing. *Arch. Rat. Mech. Anal.* **123**, 200–257 (1993)
2. Alvarez, L., Lions, P.L., Morel, J.M.: Image selective smoothing and edge detection by nonlinear diffusion II. *SIAM J. Numer. Anal.* **29**, 845–866 (1992)
3. Bänsch, E., Mikula, K.: A coarsening finite element strategy in image selective smoothing. *Computing and Visualization in Science* **1**(1) 53–61 (1997)
4. Caselles, V., Kimmel, R., Sapiro, G.: Geodesic active contours. *International Journal of Computer Vision*, **22**, 61–79 (1997)
5. Caselles, V., Kimmel, R., Sapiro, G., Sbert, C.: Minimal surfaces: a geometric three dimensional segmentation approach. *Numerische Mathematik* **77**, 423–451 (1997)
6. Chen, Y.-G. Giga, Y., Goto, S.: Uniqueness and existence of viscosity solutions of generalized mean curvature flow equation. *J. Diff. Geom.* **33**, 749–786 (1991)
7. Chen, Y., Vemuri, B.C., Wang, L.: Image denoising and segmentation via nonlinear diffusion. *J. Comput. Math. Appl.* **39**(5–6), 131–149 (2000)
8. Crandall, M.G., Ishii, H., Lions, P.L.: User’s guide to viscosity solutions of second order partial differential equations *Bull.(NS) Amer. Math. Soc.* **27**, 1–67 (1992)
9. Deckelnick, K., Dziuk, G.: Discrete anisotropic curvature flow of graphs. *RAIRO–Math. Model. Num.* **33**(6), 1203–1222 (1999)
10. Deckelnick, K., Dziuk, G.: Error estimates for a semi implicit fully discrete finite element scheme for the mean curvature flow of graphs. *Interfaces and Free Boundaries* **2**(4), 341–359 (2000)
11. Dziuk, G.: Numerical schemes for the mean curvature flow of graphs. In: Argoul, P., Frémond, M., Nguyen, Q.S. (Eds.): *IUTAM Symposium on Variations of Domains and Free Boundary Problems in Solid Mechanics*, Kluwer Academic Publishers, Dordrecht–Boston–London 63–70 (1999)
12. Evans, L.C., Spruck, J.: Motion of level sets by mean curvature I. *J. Diff. Geom.* **33** 635–681 (1991)
13. Handlovičová, A., Mikula, K., Sgallari, F.: Semi-implicit complementary volume scheme for solving level set like equations in image processing and curve evolution. *Numerische Mathematik* **93**, 675–695 (2003)
14. Kanizsa, G.: *Organization in Vision*, Praeger, New York (1979)
15. Kačur, J., Mikula, K.: Solution of nonlinear diffusion appearing in image smoothing and edge detection. *Applied Numerical Mathematics* **17**, 47–59 (1995)
16. Kichenassamy, S., Kumar, A., Olver, P., Tannenbaum, A., Yezzi, A.: Conformal curvature flows: from phase transitions to active vision. *Arch. Rational Mech. Anal.* **134**, 275–301 (1996)
17. Lin, C.J., Moré, J.J.: Incomplete Cholesky factorizations with limited memory. *SIAM. J. Sci. Comput.* **21**, 24–45 (1999)
18. Mikula, K., Ramarosy, N.: Semi-implicit finite volume scheme for solving nonlinear diffusion equations. In: *image processing, Numerische Mathematik* **89**(3), 561–590 (2001)
19. Osher, S., Sethian, J.A.: Front propagating with curvature dependent speed: algorithms based on the Hamilton–Jacobi formulation. *J. Comput. Phys.* **79**, 12–49 (1988)
20. Perona, P., Malik, J.: Scale space and edge detection using anisotropic diffusion. In: *Proc. IEEE Computer Society Workshop on Computer Vision* (1987)
21. Saad, Y.: *Iterative methods for sparse linear systems*. PWS Publ. Comp. (1996)
22. Sarti, A., Citti, G.: Subjective Surfaces and Riemannian Mean Curvature Flow Graphs. *Acta Math. Univ. Comenianae* **70**(1), 85–104 (2001)
23. Sarti, A., Malladi, R., Sethian, J.A.: Subjective Surfaces: A Method for Completing Missing Boundaries. In: *Proceedings of the National Academy of Sciences of the United States of America* **12**(97), 6258–6263 (2000)
24. Sarti, A., Malladi, R., Sethian, J.A.: Subjective Surfaces: A Geometric Model for Boundary Completion. *International Journal of Computer Vision* **46**(3), 201–221 (2002)
25. Sethian, J.A.: Numerical algorithm for propagating interfaces: Hamilton–Jacobi equations and conservation laws. *J. Diff. Geom.* **31**, 131–161 (1990)
26. Sethian, J.A.: *Level Set Methods and Fast Marching Methods. Evolving Interfaces in Computational Geometry, Fluid Mechanics, Computer Vision, and Material Science*, Cambridge University Press (1999)
27. Walkington, N.J.: Algorithms for computing motion by mean curvature, *SIAM J. Numer. Anal.* **33**(6), 2215–2238 (1996)
28. Weickert, J., Romeny, B.M.T.H., Viergever, M.A.: Efficient and reliable schemes for nonlinear diffusion filtering. *IEEE Trans. Image Processing* **7**(3), 398–410 (1998)